

Efficient Segmentation of Cell Nuclei in Histopathological Images

Oscar Cuadros Linares*, Aurea Soriano-Vargas[†], Bruno S. Façal*, Bernd Hamann[‡]
Alexandre T. Fabro[§] and Agma J. M. Traina*

*Institute of Mathematics and Computer Sciences, University of Sao Paulo, Sao Carlos, SP, BR 13566-590
Email: ocuadros@icmc.usp.br

[†]Institute of Computing, University of Campinas, Campinas, SP, BR 13083-852

[‡]Department of Computer Science, University of California, Davis, CA, U.S.A. 95616

[§]Faculty of Medicine, University of Sao Paulo, Ribeirao Preto, SP, BR, 14049-900

Abstract—Computer-aided cell nuclei segmentation in histology images is essential for image analysis. There is a demand for methods that accurately detect cell nuclei in large images. We introduce the FECS method for automatic cell nuclei segmentation in Hematoxylin and Eosin (H&E) stained histology images. Our method accurately segments cell nuclei, even in large images, efficiently. We use bimodal-like histograms to perform image binarization via the fast Otsu algorithm. We introduce a super-pixel based filter for cell nuclei boundary detection. A Gaussian blur filter allows us to identify cell nuclei centers, which are understood as local minima in the individual cell nuclei regions. We have evaluated our method for two publicly available datasets. Our tests have produced average Jaccard index values of 0.963 and 0.914, respectively, supporting a high degree of segmentation accuracy. We have compared our method against a state-of-the-art method; our method produced better results for both datasets. The average processing time of FECS was approximately just one second for images of $1k \times 1k$ pixel resolution and about three minutes for larger images of $15k \times 15k$ pixel resolution.

Index Terms—Cell nuclei, Histopathology, Segmentation, Super-pixels

I. INTRODUCTION

Histology is an area of surgical pathology in which biopsies are examined using a microscope. In everyday medical practice, examining histologic sections provides crucial information during the process of diagnosing a disease [1]. The goal is to analyze cells and tissue looking for structural and functional changes so that identifying abnormal cells, the morphology of tissue, and irregular cells organization [2]. Most diseases cause typical cell and/or tissue changes, the so-called histologic findings or patterns. To find such patterns, a pathologist usually spends hours analyzing a single biopsy sample. Commonly, this task is performed using a digitized version of the biopsy sample. When a biopsy is digitized, it may produce a very high-resolution image. For example, a digitized biopsy with $20\times$ microscope magnification may produce a digital image of size about $(110k \times 110k)$ pixels, which generates a file

The authors would like to thank FAPESP for the financial support to the project “Mining, indexing and visualizing Big Data in clinical decision support systems (MIVisBD)” (Grants 16/17078-0, 18/06074-0, 18/06228-7, and 2020/07200-9). The authors also thank the Brazilian agencies CNPq and CAPES for the promotion of scientific and technological research.

of approximately 2.0 GB [3]. Usually, a pathologist analyzes a biopsy using a lower microscope power, e.g., $5\times$, at this level, where it is possible to observe changes (patterns) in the tissue. However, those findings should be analyzed at a higher microscope power, e.g., $20\times$ looking for more specific patterns at a cellular level.

In many cases, it is not necessary to segment individual cells, since usually, pathologists are more interested in analyzing cell organization patterns instead of analyzing individual ones. Despite several methods for analyzing histopathology images have been proposed [4], [5], most of the time, this task is performed manually, i.e., pathologists do not use specialized software to aid them in finding histology patterns. The main reason is that it is extremely difficult to develop a generic method capable of identifying patterns for different diseases. For example, Interstitial Lung deceases (ILD) present characteristic patterns at a cellular level, which are found observing cell patterns and tissue changes, e.g., bronchiolitis, muscularization, and lymphoid aggregates.

In this scenario, segmenting cells in histopathological images becomes an essential first step towards disease pattern recognition. In the last years, many cell-segmentation methods have been introduced. Most of them focused on an individual cell segmentation as best as possible, i.e., segmenting the boundaries and the interior part of each cell. Even though those methods report good segmentation accuracy, they present significant limitations, such as: high processing time, are able to manage only small images, are very sophisticated approaches, which may be hard/costly to implement.

Many of these segmentation methods take advantage of the relatively well defined circular-elliptical cell shape. They apply strategies based on Laplacian of Gaussian (LoG) operators, edge detection algorithms, Hough transforms, or determinant hessian matrix, which are traditional algorithms well-known to detect circular shapes. The main limitations are excessive computation cost, high sensitivity to gray-intensity variation, and limited to detecting nearly circular cells. In this context, several related work present strategies based on an improved version of such methods. For example, Yousef Al-Kofahi et al. [6] introduced a method based on graph-cuts, the LoG

filter, and α -expansion strategy. This method first performs an automatic image binarization using a hybrid approach based on the graph-cuts algorithm and histogram image normalization. Since the graph-cuts algorithm extract connected cells, the LoG filter is applied to identify local maximum peaks, this operation is applied at multiple scales of the sigma parameter. Finally, the α -expansion and graph coloring algorithms are applied to enhance the contours between touching cells. This method presents a good accuracy in segmenting cell nuclei. Nevertheless, the main limitation of this method is its scalability. The method performs an adequate processing time only in tiny images, about 5 seconds on average.

In addition to the numerous methods available in the literature, there are some widely used by histopathologists. The reason is that those methods are implemented on available software tools for bioimage analysis [7]. For example, the method available in the QuPath software [8] applies a method based on the watershed algorithm. The method first smooths the input image using the LoG transform, and then the image background is extracted by applying a simple threshold filter. Possible cell nuclei are detected using a watershed transform. This method produces robust quality segmentation. However, it presents various limitations, e.g., parameter sensitiveness, cell size limited (different cell sizes in the same input), as well as contrast and luminance sensitiveness. Despite that, the method implemented in QuPath is a generic strategy adopted by several other methods; authors, in general, propose improvements based on this strategy [7], [9].

In this manuscript, we introduce a Fast and Efficient Cell Nuclei Segmentation (FECS) Approach for histopathological Images, focused on separating cells from tissue (foreground-background segmentation), capable of handling very large images in short processing time. The main goal of our method is to segment the entire set of cells nuclei found in histology images stained with Hematoxylin-Eosin (H&E). Besides, we label individual cell nuclei centroids, which facilitates applying posterior tasks, such as detecting cell clusters, computing cell clusters shape, and counting cells; measurements that are useful to find various disease patterns. Our method takes advantage of the bimodal-like histograms to apply a fast binarization using the Otsu algorithm and a super-pixels algorithm to detect cell nuclei boundaries. Finally, we identify cell nuclei centroids by applying a Gaussian blur filter integrated into the proper pixel value of the CIELAB color model, considering the type of images. Besides the high segmentation accuracy of FECS, we highlight that we do not apply any post-process, e.g., filling holes, smoothing boundaries, or disjointing combined cells in one region. FECS presents linear-complexity, which makes it suitable for segmenting cells in large images.

II. METHOD

The diagram of Fig. 1 illustrates the method FECS proposed in this paper.

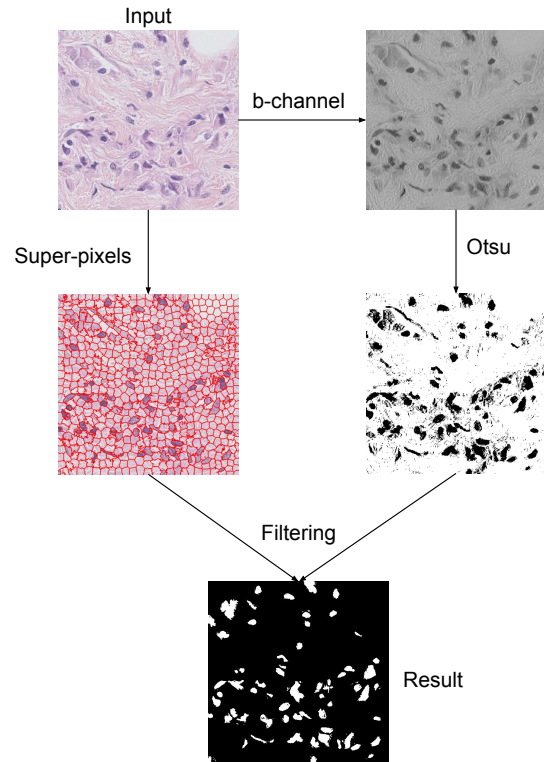


Fig. 1: Proposed FECS method diagram. We convert the RGB input image into a CIELAB version of it, and then we extract the b -channel. The Otsu algorithm is then computed using the b -channel as input. Meanwhile, we apply the super-pixels algorithm on the input image. Next, we apply our super-pixels filter to extract the cell nuclei from the Otsu output.

A. Hematoxylin-Eosin stain and the CIELAB color model

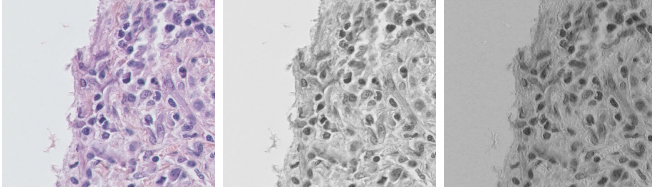
The Hematoxylin-Eosin (H&E) is a stain capable of highlighting the fine structures of cells and tissues. It has become the standard stain for histologic examination of human tissues. In our application, the main advantage of H&E stain is that the primary colors of cell nuclei are within a scale of blue or dark-purple, whereas other tissues such as collagen or extracellular matrix are stained in a scale of pink [1]. From an image analysis point of view, this feature allows that locally the cell nuclei are always darker than surrounding tissue.

Most computer analysis methods perform using the RGB color model or a gray-scale version computed from it. The main limitation of using RGB is that it is susceptible to illumination or contrast irregularities, and it is tough to deal with that. Besides, RGB is an additive color model, where the primaries red, green, and blue are added together to reproduce other colors. The problem with this model is that it is not intuitive to compute the difference among them, e.g., using the Euclidean distance with RGB triplets does not allow to clearly define color differences [2].

To overcome such limitations, we transform the input RGB channels into CIELAB triplets. The CIELAB color model represents colors as three values: L for the lightness from

black (0) to white (100), a from green (-) to red (+), and b from blue (-) to yellow (+). The main advantage of this model is that it is possible to adjust the lightness contrast using the L component or compute color distances using the a and/or b components.

Besides, we noticed most cell nuclei information are contained in the b component (blue to yellow), contrasts within cells are more regular (compared with RGB gray-scale), and cell nuclei boundaries are well preserved. Thus, we extract the b channel to perform our cell nuclei segmentation method on it. In Fig. 2c, we show a comparison between the b channel and the RGB gray-scale.



(a) Input RGB image (b) RGB gray-scale (c) b -Channel

Fig. 2: Comparison between RGB gray-scale and CIELAB b -channel. Since in the b -channel, there is no luminance information, possible irregularities on it are eliminated. Besides, the contrast between cell nuclei and surrounding tissue are well preserved. Notice in this example we have rescaled (0-255) the b -channel pixel values for visualization purposes.

B. Image binarization

Background and foreground segmentation are the first steps in many cell nuclei segmentation methods [10]. The goal of this step is to coarsely segment all cells (foreground) from other materials, such as: tissue and image background. Several methods could be applied, e.g., thresholding and graph-cuts. In our application, we conjecture that histopathological images present bimodal histograms since cell nuclei appear darker than the surrounding areas. Therefore, a suitable strategy to binarize this type of image is applying the Otsu algorithm. Otsu finds a global threshold that minimizes the weighted intra-class variance, and it is analogous to a globally optimal k-means [11]. The intra-class variance relation is given by:

$$\sigma_w^2(t) = q_1(t)\sigma_1^2(t) + q_2(t)\sigma_2^2(t), \quad (1)$$

in which q_1 and q_2 are the probabilities of two classes being separated by the threshold t , and σ_1^2 and σ_2^2 are the respective class variance. The class probability is computed as:

$$\begin{aligned} \sigma_1^2(t) &= \sum_{i=1}^t [i - \mu_1(t)]^2 \frac{P(i)}{q_1(t)}, \\ \sigma_2^2(t) &= \sum_{i=t+1}^L [i - \mu_2(t)]^2 \frac{P(i)}{q_2(t)}, \end{aligned} \quad (2)$$

where L are the bins of the image histogram, the class means μ and variance weights are defined as:

$$\begin{aligned} q_1(t) &= \sum_{i=1}^t P(i), \quad \text{and} \quad q_2(t) = \sum_{i=t+1}^L P(i), \\ \mu_1(t) &= \sum_{i=1}^t \frac{iP(i)}{q_1}, \quad \text{and} \quad \mu_2(t) = \sum_{i=t+1}^L \frac{iP(i)}{q_2}. \end{aligned} \quad (3)$$

where b are b -channel pixels values. After computing the threshold t , it is used to generate a binary image B by applying a simple thresholding filter on the b -channel.

Since H&E-stained cells are darker than surrounding tissue, Otsu becomes a suitable algorithm to binarize such images. In addition, since we use the b -channel, problems with contrast are significantly reduced, which minimizes the amount of wrongly labeled pixels. In spite of that, Otsu's output may present some imperfections, i.e., pixels wrongly labeled as foreground (cells). We address this problem by applying a super-pixel filter described in the next section. In Fig. 4b, we show an example of the Otsu algorithm applied to a histopathological image.

C. Super-pixels

Super-pixels is a region-based technique that segments an image into groups of pixels that share a similar color and are in a neighboring position. One of the main advantages of super-pixels is that they identify image boundaries very accurately, which is desirable in our application. Several approaches for super-pixels have been proposed [12]. We implemented a CIELAB-based version of the super-pixel algorithm, called Speeded-up turbo pixels (SUTP) [13], which is efficient and straightforward, and produces super-pixels well fitted to image boundaries.

The SUTP method is based on the k-means clustering algorithm. The first step consists of dividing the image Ω into N regular super-pixels Ω_I ($I \in N$), with edge length l . Initially, all super-pixels have the same area and equidistant centroids. Without loss of generality, we assume that the input image has a square shape. During the second step, pixels along a specific super-pixel boundary (\mathbf{x}_i) are analyzed and possibly shifted across the border between neighboring super-pixels. This pixel-swapping is applied iteratively, and it is based on this cost function to be minimized:

$$C_{i,I} = p_1 \|\Omega_i - \Omega_I\|^2 + p_2 \|\mathbf{x}_i - \mathbf{x}_I\|^2, \quad (4)$$

where Ω_I is the CIELAB mean (a vector of three components, lab) of the I^{th} super-pixel, and \mathbf{x}_I is the spatial centroid of the I^{th} super-pixel. The parameters p_1 and p_2 are weights for color similarity and super-pixel border rigidity, respectively. "More convex" super-pixels are generated for high values of p_2 , although super-pixels may not accurately fit to object boundaries. Determining near-optimal values for p_1 and p_2 depends on the application. In our method, super-pixels adjusted well to boundaries are preferable to convex ones. Hence, we use the values $p_1 = 1$, $p_2 = 0.5$, and the number of iterations is chosen as $it = 5$, as suggested in [14]. Defining the initial

size of the super-pixels l also depends on the application, in Section III we give all parameter setup. Fig. 3 shows the super-pixels after convergence.

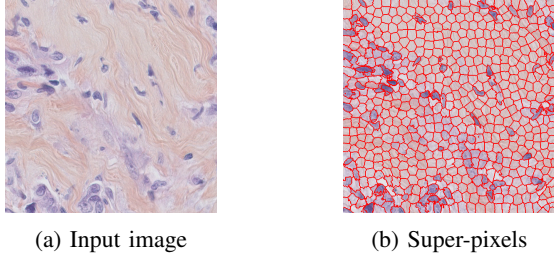


Fig. 3: Super-pixels convergence. Notice super-pixels are well fitted to the cell nuclei boundaries.

D. Foreground and super-pixels based filter

Dividing the input image into background and foreground (cells), allows extracting the entire set of cell nuclei. However, many pixels may wrongly be labeled, as shown in Fig. 4b. We address this problem by applying a threshold-based filter in which we match both the super-pixels and the Otsu outputs, and if the number of pixels in Otsu is greater than a threshold, we label that super-pixel as being cell nuclei. By applying this filter, not only wrongly labeled pixels are corrected, but also super-pixels containing cell nuclei are segmented. This filter is defined as follows:

$$I_l = \begin{cases} 1, & \delta(I, B) > t, \\ 0, & \text{otherwise} \end{cases}, \quad (5)$$

where I_l is the label of the l^{th} super-pixel, $l \in \{0, 1\}$, function δ returns the percentage of pixels in B within the super-pixel I , and t is a threshold value that, empirically, should be greater than 50%. After applying this filter, all super-pixels whose label is equal to 1 are defined as cell nuclei super-pixels. In Fig 4, we show an output example of this filter.

E. Cell nuclei local minimum

An additional step of our method consists of identifying cell nuclei local minimum, defined as flat zones surrounded by pixels of higher value. The goal of this process is to detect individual cell nuclei centers. This allows to computing measurements, such as the number of cells, distance among cells, finding clusters, and others. To detect peaks within cells, we apply a Gaussian blur filter on the set of segmented cells using the corresponding pixel value in the b -channel, as shown in Fig. 5.

III. RESULTS AND VALIDATION

We have evaluated our FECS method for two publicly available and representative datasets of H&E stained images with available ground truth (GT) data. The first dataset, called TNBC, is a collection of 50 annotated histology images of resolution 512×512 , scanned at $40\times$ microscope magnification. Each image was taken from a cohort of 11 triple-negative

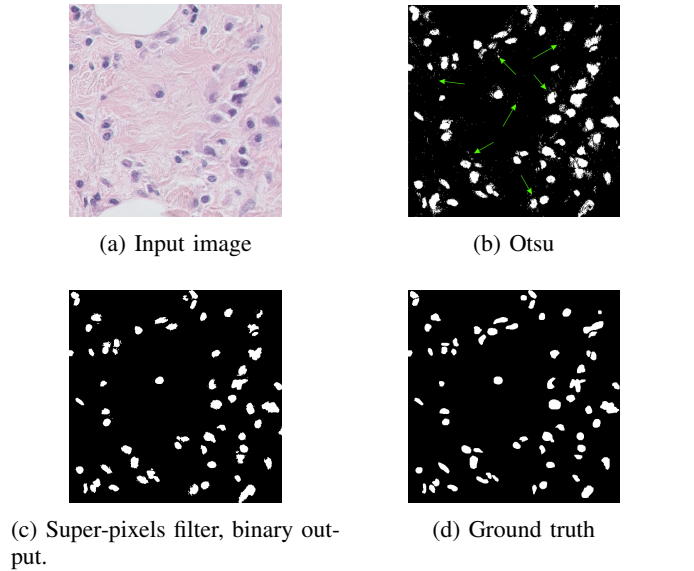


Fig. 4: Image filtering using super-pixels. Wrongly labeled pixels, (green arrows) are eliminated by applying the filter.

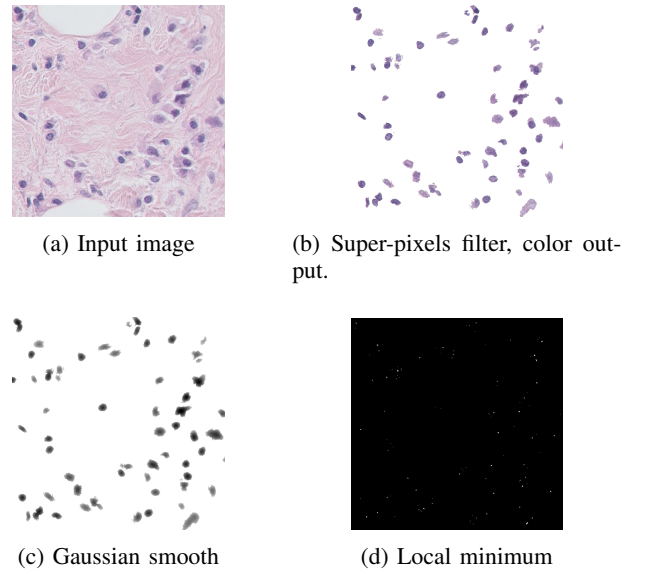


Fig. 5: Cell nuclei centers are identified by finding local minimum points. We apply a Gaussian smoothing on the super-pixels filter output using the b -channel pixel values.

cancer patients [15]. The second dataset, called MoNuSeg, is a collection of 44 images of resolution 1000×1000 , scanned at $40\times$ microscope power. This dataset provides images for these organs: breast, liver, kidney, prostate, bladder, colon, and stomach; including benign and diseased tissue [16].

We carried out our experiments on a Linux workstation (Intel Core i7-2600 CPU 3.40GHz x 4, with 16GB memory). We implemented our method in C++ and used the National Library of Medicine Insight Segmentation and Registration Toolkit (ITK) [17].

Table I presents the parameters used in our experiments.

The super-pixels algorithm requires a user to define four parameters, see Section II-C; optimal parameter values depends on the application. In [14] value settings for these parameters were evaluated. We used values for the parameters p_1 and p_2 as suggested in that publication. Initial super-pixel size l and number of iterations it are correlated: $it = \frac{l}{2}$.

TABLE I: Parameters values for Otsu, Super-pixels (SP), Super-pixel filter (SPF), and Gaussian blur (GB).

Method	Parameter	Value
Otsu	$bins$	100
SP	p_1	1
SP	p_2	0.5
SP	l	20
SP	it	10
SPF	t	60%
GB	σ	5

To quantitatively evaluate the accuracy of our method, we have compared our segmentation results with their corresponding GT. We have measured the similarity between them by using the Jaccard index, a metric commonly used in medical image segmentation. We have compared our segmentation results against those produced by the QuPath method version 0.1.2, using the eight parameters by default advised by the authors. Fig 6 shows the Jaccard index curves of the QuPath and FECS methods. Table II presents the average Jaccard index values.

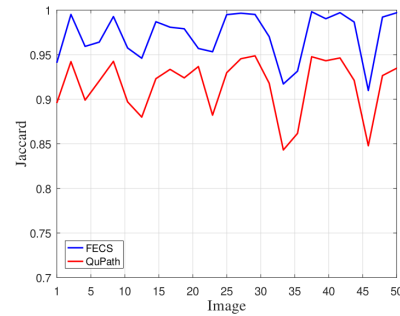
TABLE II: Jaccard index mean and standard deviation of QuPath and FECS methods for TBNC and MoNuSeg datasets.

Method	TBNC		MoNuSeg	
	Mean	Std Dev	Mean	Std Dev
FECS	0.963	0.029	0.914	0.030
QuPath	0.906	0.033	0.873	0.031

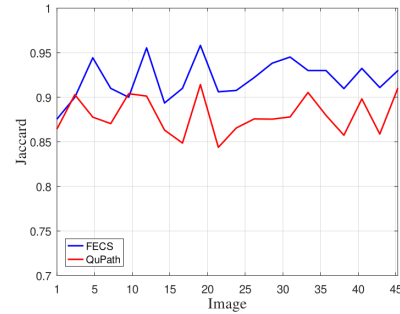
We observed that, in most cases, Jaccard index values are high, i.e., > 0.9 , for both methods. This fact is indicative of high segmentation quality. The Jaccard index curves for both methods are very similar; nevertheless, FECS performs better than QuPath in most cases. Our team, including a histopathology specialist, has visually analyzed the segmentations produced; the FECS results satisfied the specialist’s segmentation quality criteria. Fig. 7 provides a visual example of two segmentation results produced by the QuPath and FECS methods.

In addition to using the Jaccard index and a specialist’s visual inspection of results, we computed precision and recall values for both methods (FECS and QuPath), using the TNBT and MoNuSeg datasets; they are two good indices to measure segmentation quality based on true positives (cells identified as cells), false positives (non-cells identified as cells), and false negatives (cells not identified as cells). Results are provided in Table III.

Precision and recall values for the segmentations of both datasets are significantly better for our method, FECS. The



(a) TBNC dataset



(b) MoNuSeg dataset

Fig. 6: Jaccard index curves for FECS and QuPath. Our proposed FECS method performs better than the QuPath method in most cases; however, both methods produce high Jaccard index values.

TABLE III: Precision and recall means of QuPath and FECS for TBNC and MoNuSeg datasets.

Method	TBNC		MoNuSeg	
	Precision	Recall	Precision	Recall
FECS	0.862	0.837	0.897	0.855
QuPath	0.655	0.740	0.544	0.757

generated results confirm that our method is capable of covering most of the cells in the images, with image noise having hardly any effect.

Finally, we evaluate the scalability of FECS on a dataset of 72 histology images scanned at $5\times$ microscope magnification, images of about $15k \times 15k$ pixel resolution. The average time processing FECS segmented those images was three minutes with a single processor implementation. We do not provide a comparison with QuPath since it cannot process images of this size. Since there is no GT available for this dataset, in Fig 8, we show an example of a segmentation result.

IV. CONCLUSIONS

We introduced a highly efficient method, FECS, for cell nuclei segmentation for histopathological images. We validated our approach using two datasets, TNBC and MoNuSeg, and three evaluation metrics: Jaccard index, precision, and recall. Further, we compared our results with those generated by another approach that is commonly used by pathologists. Our results demonstrate that our method produces a more accurate

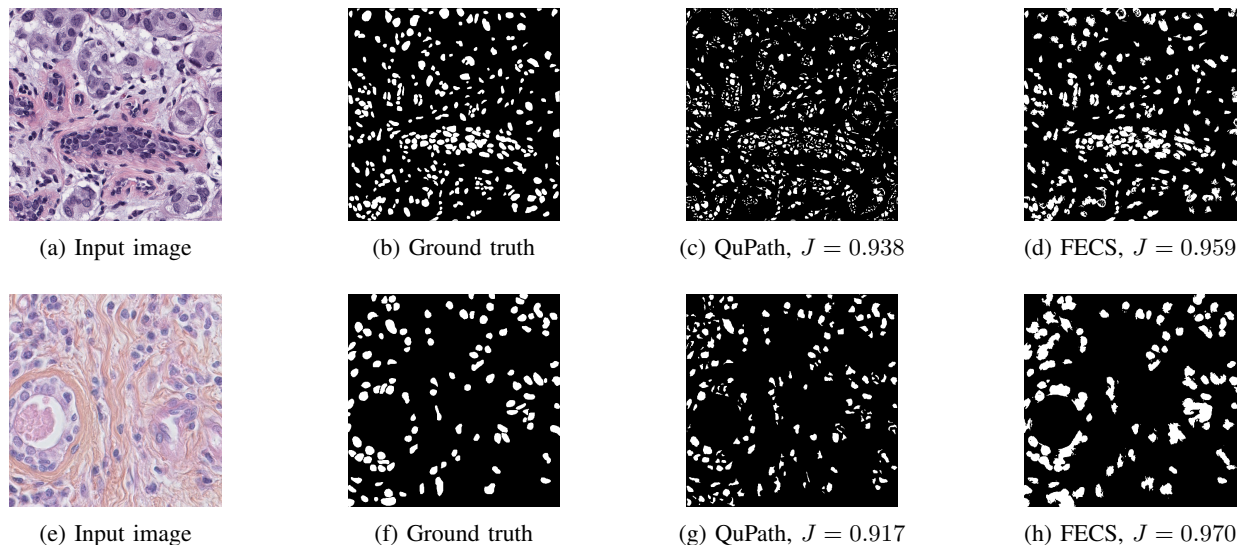


Fig. 7: Visual comparison of QuPath and FECS methods. Both methods produce high Jaccard index (J) values, according to a specialist. The main problem of QuPath is over-segmentation. FECS detects all entire cell nuclei in nearly all cases.

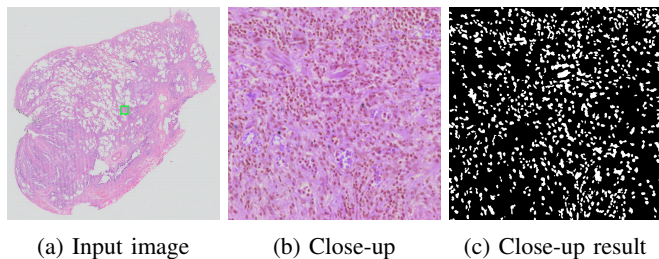


Fig. 8: Cell nuclei segmentation example of an image of $15k \times 15k$ pixel resolution. In (b) a close-up view of the green frame in (a).

segmentation of cell nuclei than this alternative method. Besides, our method is generating results for very large images in short processing time. These facts make our method useful for real-world medical image analysis and interpretation.

Concerning future work, we intend to implement a multi-processor version of FECS and make it publicly available. We also intend to use the FECS segmentation to identify disease patterns at the cellular level in combination with machine learning techniques to aid in the disease diagnosis process.

REFERENCES

- [1] J. K. Chan, "The wonderful colors of the hematoxylin–eosin stain in diagnostic surgical pathology," *Int. J. of Surgical Pathology*, vol. 22, no. 1, pp. 12–32, 2014.
- [2] K. Kuru, "Optimization and enhancement of h&e stained microscopical images by applying bilinear interpolation method on lab color mode," *Theoretical Biology and Medical Modelling*, vol. 11, no. 1, p. 9, 2014.
- [3] O. Cuadros Linares, B. Faiçal, P. Barbosa, B. Hamann, A. Fabro, and A. Traina, "How to automatically identify regions of interest in high-resolution images of lung biopsy for interstitial fibrosis diagnosis," in *IEEE 32nd International Symposium on Computer-Based Medical Systems (CBMS)*, June 2019, pp. 571–574.
- [4] A. Belsare and M. Mushrif, "Histopathological image analysis using image processing techniques: An overview," *Signal & Image Processing*, vol. 3, no. 4, p. 23, 2012.
- [5] B. S. Deshmukh and V. H. Mankar, "Segmentation of microscopic images: A survey," in *Int. Conf. on Electronic Systems, Signal Processing and Computing Technologies*, 2014, pp. 362–364.
- [6] Y. Al-Kofahi, W. Lassoued, W. Lee, and B. Roysam, "Improved automatic detection and segmentation of cell nuclei in histopathology images," *IEEE Trans. on Biomedical Engineering*, vol. 57, no. 4, pp. 841–852, 2009.
- [7] R. Paulik, T. Micsik, G. Kiszler, P. Kaszál, J. Székely, N. Paulik, E. Várhalmi, V. Prémusz, T. Krenács, and B. Molnár, "An optimized image analysis algorithm for detecting nuclear signals in digital whole slides for histopathology," *Cytometry Part A*, vol. 91, no. 6, pp. 595–608, 2017.
- [8] P. Bankhead, M. B. Loughrey, J. A. Fernández, Y. Dombrowski, D. G. McArt, P. D. Dunne, S. McQuaid, R. T. Gray, L. J. Murray, H. G. Coleman *et al.*, "Qupath: Open source software for digital pathology image analysis," *Scientific reports*, vol. 7, no. 1, pp. 1–7, 2017.
- [9] S. Li, L. Wu, and Y. Sun, "Cell image segmentation based on an improved watershed transformation," in *Int. Conf. on Computational Aspects of Social Networks*, Sep. 2010, pp. 93–96.
- [10] M. Abdolhoseini, M. G. Kluge, F. R. Walker, and S. J. Johnson, "Segmentation of heavily clustered nuclei from histopathological images," *Scientific reports*, vol. 9, no. 1, pp. 1–13, 2019.
- [11] N. Otsu, "A threshold selection method from gray-level histograms," *IEEE Trans. on Systems, Man, and Cybernetics*, vol. 9, no. 1, pp. 62–66, 1979.
- [12] D. Stutz, A. Hermans, and B. Leibe, "Superpixels: An evaluation of the state-of-the-art," *Computer Vision and Image Understanding*, vol. 166, pp. 1–27, 2018.
- [13] C. Çiğla and A. A. Alatan, "Efficient graph-based image segmentation via speeded-up turbo pixels," in *IEEE Int. Conf. on Image Processing*, 2010, pp. 3013–3016.
- [14] O. C. Linares, B. Hamann, and J. B. Neto, "Segmenting cellular retinal images by optimizing super-pixels, multi-level modularity, and cell boundary representation," *IEEE Trans. on Image Processing*, vol. 29, pp. 809–818, 2019.
- [15] P. Naylor, M. Laé, F. Reyat, and T. Walter, "Nuclei segmentation in histopathology images using deep neural networks," in *IEEE 14th Int. Symp. on Biomedical Imaging (ISBI)*, 2017, pp. 933–936.
- [16] N. Kumar, R. Verma, S. Sharma, S. Bhargava, A. Vahadane, and A. Sethi, "A dataset and a technique for generalized nuclear segmentation for computational pathology," *IEEE Trans. on Medical Imaging*, vol. 36, no. 7, pp. 1550–1560, 2017.
- [17] H. J. Johnson, M. M. McCormick, and L. Ibanez, "The itk software guide book 1: Introduction and development guidelines fourth edition updated for itk version 4.7," *Kitware, Inc.(January 2015)*, 2015.